CHEMICAL AND ELECTRICAL CHARACTERIZATION OF N- AND P-TYPE MULTI-CRYSTALLINE SOLAR GRADE SILICON WAFERS

M. Di Sabatino[1*], S. Binetti[2], E. J. Øvrelid[1], M. Acciarri[2], J. Libal[2]
[1]SINTEF, Materials and Chemistry, A. Getz v. 2B, 7465 Trondheim (Norway)
[2] Università di Milano-Bicocca (UNIMIB), Dept. of Materials Science, via Cozzi 53, 20125 Milano (Italy)
Email:marisa.di.sabatino@sintef.no

ABSTRACT: Due to the shortage of feedstock, the photovoltaic industry is looking for new and less expensive sources of material. Metallurgical based materials could be a solution, but usually contain higher levels of impurities and they often tend to be n-type. The interest for solar cells based on n-type silicon wafers is steadily growing due their lower sensitivity to carrier lifetime degradation compared to p-type silicon based solar cells. In this study, we have investigated two multicrystalline (mc) silicon wafers (n- and p- type) cut from ingots grown from feedstock from a direct metallurgical route. The aim of this work is to study, by combination of different techniques, the defects and impurities interaction and their recombination properties in mc-Si grown using low quality silicon feedstock. The results show that for the material investigated a single directional solidification step might be sufficient to reduce the metallic impurity concentration to values compatible with solar application. N- and p-type wafers have shown similar electrical properties.
Keywords: Multicrystalline Silicon, Metallurgical Silicon, Impurities, Carrier Recombination, Dislocation Density.

1 INTRODUCTION

The photovoltaic (PV) industry is growing at a much faster rate than the silicon feedstock supply. Therefore, PV industry is currently facing a silicon feedstock shortage. In order to solve this problem, in the past years great attention has been given to lower quality solar-grade (SoG) silicon feedstock to produce cost effective solar cells and also to wastes from the electronic market which produces approximately 200 tons/year of n-type silicon material (single crystalline silicon, sc-Si). There are two major consequences of this phenomenon, namely a higher amount of impurities accompanying the starting material for solar cell production and interest in producing n-type multicrystalline silicon (mc-Si) wafers.

N-type mc-Si has some remarkable advantages. Firstly, there are little or no boron-oxygen complexes and the lifetime of minority carriers does not decrease with the injection level [1, 2]. Secondly, the minority carrier capture cross sections of metallic impurities found in silicon material are markedly smaller for holes (which are the minority carries for n-type) than for electrons (which are minority carries for p-type) [1, 3]. The great interest in n-type silicon solar cell is also fed from the experimental results which have recently reported exceptional values of the electron lifetime (>hundreds µs in raw materials and even larger for gettered wafers) [2, 4, 5, 6].

Despite the use of lower quality silicon feedstock to answer the market demand, impurities are expected to be detrimental for the efficiency of the solar cells. Furthermore, interaction between impurities and extended defects affects the recombination rate of minority carries in the wafers and, hence, the electrical properties and the efficiency of the solar cells.

The aim of this work is to study, by combination of different techniques, the defects and impurities interaction and their recombination properties in mc-Si grown using low quality silicon feedstock. The knowledge of the defects and impurities interaction and of their recombination strength is of fundamental importance in order to reduce their influence on solar cell efficiency.

2 EXPERIMENTAL

2.1 Casting experiment and wafering

A mc-Si ingot was grown using feedstock from a direct metallurgical route in a directional solidification furnace at SINTEF Materials and Chemistry. The charge material was approximately 12 kg of metallurgical grade (MG) silicon. Details of the furnace and casting experiments were previously given [7]. The ingot was cut into 50x50x100 mm bricks. One of the bricks was cut as shown in Figure 1.

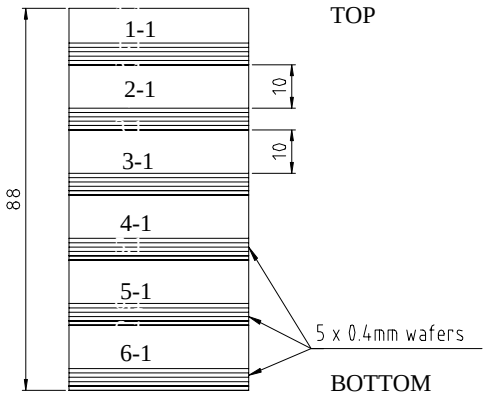

Figure 1: Schematic view of the brick cut in six slices and thirty wafers

The brick was divided in six 10 mm thick slices (1-1, 2-1, 3-1, etc.) and the rest was wire-sawed into thirty 400

µm thick wafers (1-2, 1-3, 1-4, 2-2, 2-3, 2-4 etc). Chemical analysis by Glow Discharge Mass Spectrometer (GD-MS, *see poster by M. Di Sabatino et al. at this conference*) was performed on the thick slices in order to monitor the distribution of the impurities along the brick from bottom to top.

All wafers were mechanically polished. For dislocation density analysis the samples were etched with Sopori etching, while for EBIC and PL measurements, the wafers were chemically polished with CP4 ($HF:HNO_3:CH_3COOH$=3:5:3 volume ratio).

2.2 Experimental techniques

In order to map the grains and grain boundaries, Scanning Electron Microscopy-Electron BackScattered Diffraction (SEM-EBSD) was performed on the selected wafers with Zeiss SUPRA 55Vp. This technique gives also a map of the orientation of the grains as well as their coincidence site lattice (CSL).

Dislocation density analysis was carried out with GT-PVscan 6000 at a resolution of 50 µm on the parallel wafers used for EBSD analysis.

Electron Beam Induced Current (EBIC) measurements at room temperature were carried out on the selected wafers. The EBIC measurements were carried out with a Vega TS5136 XM Tescan Scanning Electron Microscope equipped with an EBIC apparatus. The electron beam excitation was fixed at 25 kV and the beam current was kept below 10 pA. A quantitative analysis of the recombination activity of extended defects was obtained using the EBIC contrast (C) defined by:

$$C=(I_b-I_g)/I_b$$

where I_b and I_g are the EBIC currents in the bulk and at the defect, respectively [8].

Photoluminescence (PL) measurements were carried out to get supplementary information on radiative recombination processes occurring under illumination. The PL spectra were recorded at 14 K with a spectral resolution of 6.6 nm, using an InGaAs detector and a quantum well laser (λ=805 nm) as excitation source.

The interstitial oxygen $[O]_i$ and substitutional carbon $[C]_s$ content were determined by Fourier Transform InfraRed (FT-IR) spectroscopy in the 400-4000 cm^{-1} range, at room temperature [9, 10]. The total oxygen content was measured by LECO [11].

The Hall mobility [12] was determined at room temperature (magnetic field of 5000 Gauss) using the van der Pauw geometry on the samples already prepared for EBIC measurements. Ohmic contacts were obtained depositing InGa paste on the four sample corners.

A four point probe technique [13] was also used to measure the homogeneity of the resistivity measurements in the wafers.

3 RESULTS AND DISCUSSION

The results of the GD-MS analysis are shown in Figure 2. The first slice (1-1) which is close to the top of the ingot (approximately 88 mm distance from the bottom) has the highest amount of impurities, as one may expect. The P content is about 4.62 ppmw, while B, Al and Fe concentrations are 1.87, 1.18 and 0.09 ppmw, respectively. The concentrations of other trace elements such as Cu, Ni and Ti, is less than 50ppbw.

The results of the EBSD analysis are shown in Figure 3. It is possible to observe that the grain size of the two mc-Si wafers is similar, ranging from a few mm up to 10 mm, approximately. The grain orientation is marked by different colors (see colored orientation legend in Fig. 3c).

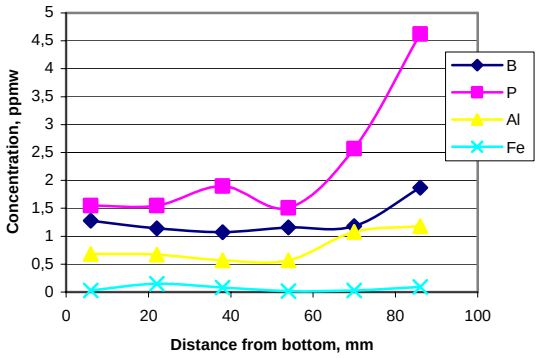

Figure 2: Chemical composition of the thick slices at different positions (distance from bottom)

Table I shows the values of the resistivity, the Hall mobility and the density of the majority charge carriers measured on two wafers (1-2 and 2-2) and two reference materials (n- and p- type sc-Si). Two areas for each wafer are selected (1-2-B and C, 2-2-A and B). The wafers 1-2 and 2-2 are n- and p- type, respectively. The mobility values are much lower in mc-Si that in sc-Si, as one may expect, due to the presence of extended defects.

Table I: Resistivity, electrical mobility and majority charge carrier density

Sample	Resistivity (Ohm cm)	Mobility (eV/cm^2s)	Carrier Density (cm^{-3})
1-2B n-type	1.89±0.01	286±9	$(1.1\pm0.1)x10^{16}$
1-2C n-type	1.71±0.03	233±9	$(1.6\pm0.1)x10^{16}$
2-2A p-type	5.24±0.05	112±1	$(1.1\pm0.1)x10^{16}$
2-2B p-type	5.78±0.05	104±1	$(1.0\pm0.1)x10^{16}$
Sc n-type	1.23±0.05	1410±10	$(3.4\pm0.3)x10^{15}$

Sc p-type	2.01±0.01	340±3	(9.1±0.1)x10^{15}

Moreover, these data are significantly lower than mc-Si ingot grown using waste feedstock [14] (*see poster by J. Libal et al. at this conference*). The low mobility values measured are probably due to the reduced dimension of grains and, therefore, to the higher influence of grain boundaries on the carrier transport properties.

Dislocation density measurements by PVscan for wafers 1-6 and 2-6 (parallel to 1-2 and 2-2) are shown in Figure 4. From these measurements it was possible to determine a dislocation density up to 1.2 10^6 cm^{-2} in the worst regions.

Figures 5 and 6 report two examples of EBIC images at low and high magnification for each wafer (1-2 and 2-2, respectively). EBIC images at high magnification were used to measure the defect contrast (at GBs and dislocations). Within these two samples, two areas were selected (1-2C and 2-2A, respectively) because they had grains with similar orientation (see EBSD map in Fig. 3). The misorientation angle between these two grains (yellow and green grains in Fig. 3) is approximately 57 degrees. Both samples had high GB contrasts (between 15% and 70%). The dislocation contrasts at room temperature were between 6% and 8% for both samples but different dislocations reveal very high contrast (20%). The sample 1-2C had higher recombination activity of dislocations than sample 2-2A. The strong dislocation and GB activity at room temperature is indicative of a high decoration by impurities (metals) [15, 16]. As one may expect, close to the top of the mc-Si ingot (sample 1-2C) a higher concentration of impurities gave higher recombination activity of dislocations. The samples selected for EBIC characterization contain grains with similar orientation (grains yellow and green in the EBSD maps). The EBIC analyses show that, for both wafers, grains with similar orientation (green grains) may have similar density of active dislocations. Further investigations are needed to prove this result. Transmission Electron Microscopy (TEM) study of impurities distribution on this material is also presented at this conference (see poster by H. Nordmark et al.).

From the EBIC maps it was also possible to calculate the density of active dislocations in these samples. A dislocation density of 10^6 cm^{-2} was measured in the worst regions in agreement with the PVscan measurements.

The measurements of the PL spectra were carried out on both samples 1-2 and 2-2, and the results are shown in Figure 7. The PL spectrum of sample 2-2A shows two lines at 0.77 and 0.93 eV which usually are known as P- and H- line, respectively [17, 18]. These lines are related to the presence of C-O complex and nuclei of SiO_x, known as old thermal donors (OTD). However, the FT-IR measurements in Table II show that the samples have similar $[O]_i$ and $[C]_s$ concentrations. The total amount of oxygen in the two wafers was measured by LECO and is 29 and 32 ppma, respectively. This result reveals that most of the oxygen was present as interstitial but there were approximately 5 to 8 ppma oxygen present as precipitates (*see poster by H. Nordmark et al. at this conference*). These results are in agreement with the presence of P- and H- lines in the PL spectrum of sample 2-2.

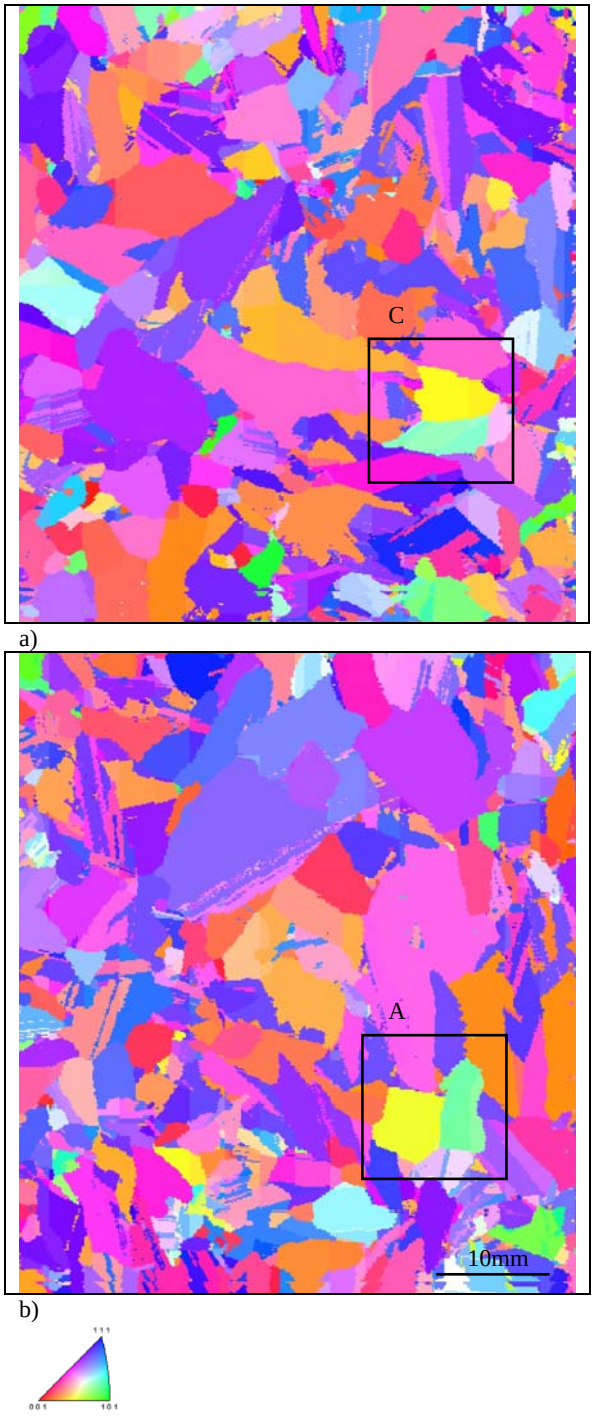

Figure 3: Electron Back Scattered Diffraction micrographs for wafers 1-2 (a) and 2-2 (b). The colored orientation legend is also shown (c)

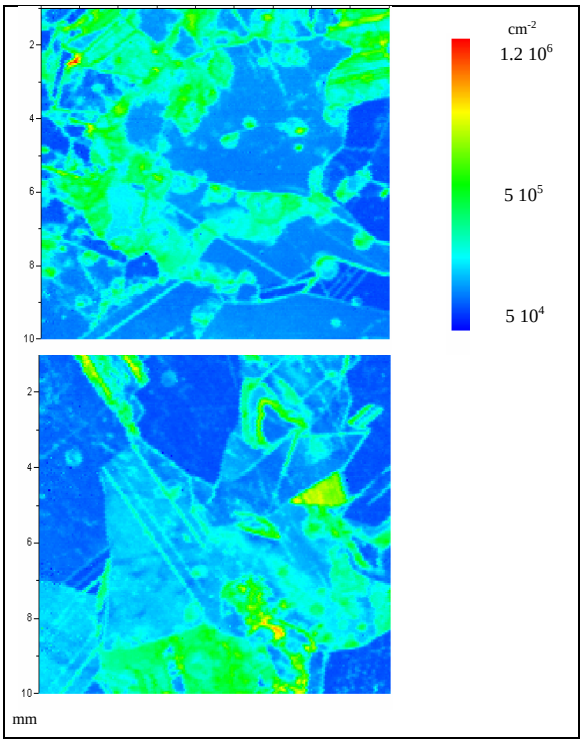

Figure 4: Dislocation density measurements for wafers 1-6 (parallel to 1-2 and in the same area of 1-2C) (a) and 2-6 (parallel to 2-2 and in the same area of 2-2A) (b). The scale of the dislocation density measurements (cm^{-2}) is also shown

Table II: Interstitial oxygen $[O]_i$ and substitutional carbon $[C]_s$ concentrations (ppma)

Sample	$[O]_i$	$[C]_s$
1-2	23.5±0.5	9.6±0.5
2-2	24.4±0.5	6.9±0.5

As the P line luminescence should be related to a transition from a thermal donors (TD-) bound excitation level to a deep level corresponding to the C-O complexes [19, 20], it could be responsible for a decrease of the carrier-lifetime. However, these complexes could be dissolved by an annealing at 650 °C for 15 min. Furthermore, an intense peak at about 1.05 eV is present in both spectra. This peak is often observed in compensated mc-Si and is probably related to a transition involving dopant levels [21]. However, taking into account the energetic position of this emission, one or two shallow levels should be involved, and the related defects should play, therefore, a negligible role in lifetime losses.

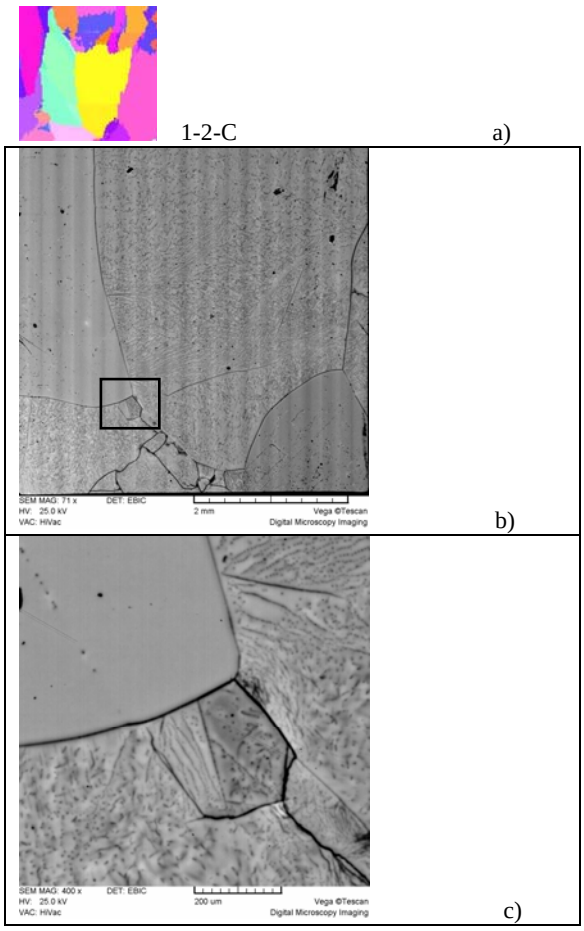

Figure 5: EBIC maps of sample 1-2C (a) at low (b) and high (c) magnification

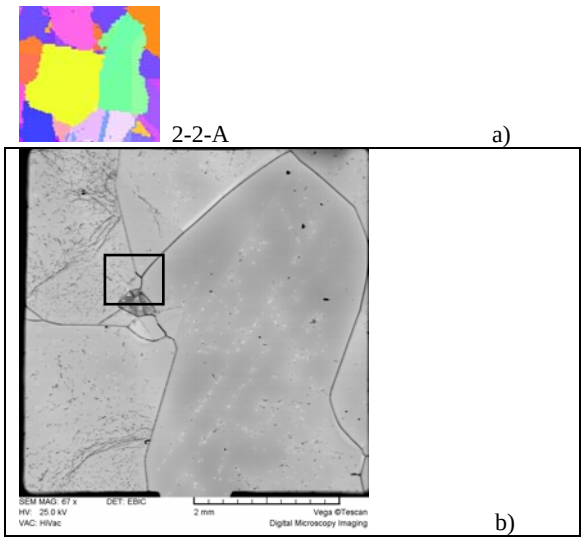

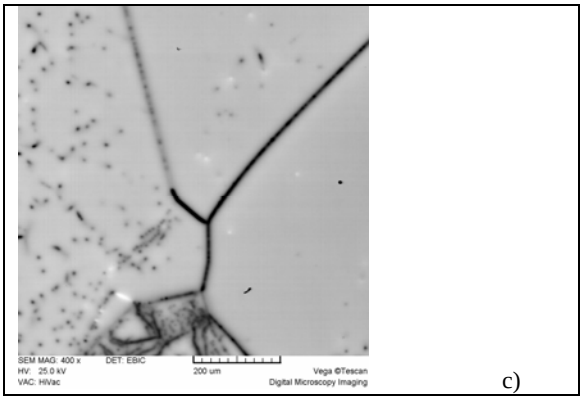

Figure 6: EBIC maps of sample 2-2A (a) at low (b) and high (c) magnification

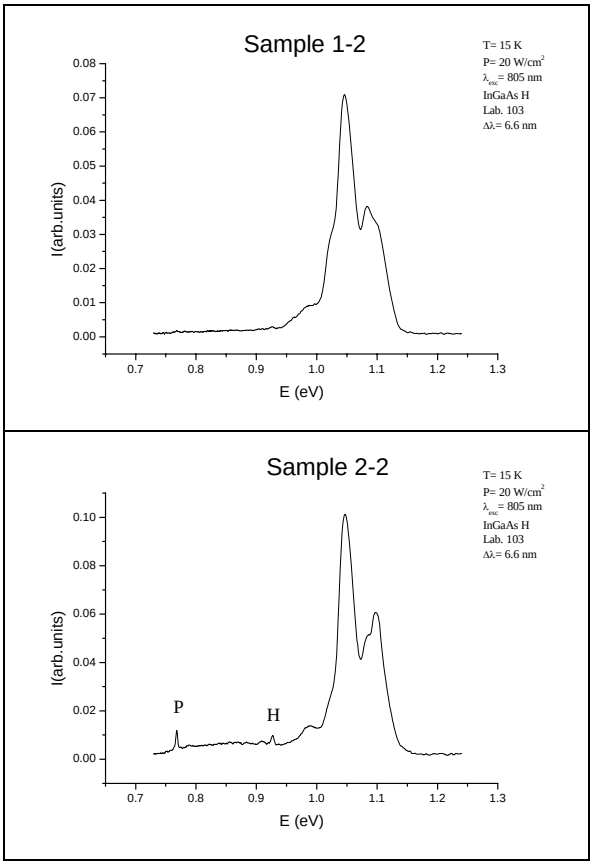

Figure 7: PL spectra of wafers 1-2 and 2-2

4 CONCLUSIONS

An investigation on the quality of mc-Si grown from metallurgical grade silicon feedstock has been carried out.

The material was compensated and we have investigated and compared the electrical properties of two wafers, n- and p- type.

The results have shown that for this material a single directional solidification step might be sufficient to reduce the metallic impurity concentration to values compatible with solar cells applications (for example a Fe concentration below to 0.09 ppmw). Metallic impurities are dissolved in the matrix or have decorated extended defects (dislocations and grain boundaries). However, taking into account the well known gettering effect of P-diffusion step on dissolved metals (phosphorus gettering), we are confident that the electrical properties of the material, hence the solar cell efficiency, can be improved during the solar cell process.

The relatively reduced dimension of grains could be a limiting factor for the mobility but it could be expected that larger ingots will reduce this problem.

The data and information obtained by this work will be used for optimizing the solar cell process for this material which is currently in progress.

ACKNOWLEDGEMENTS

The European project FoXy-Development of solar-grade silicon feedstock for crystalline wafers and cells by purification and crystallisation (SES6-019811) is gratefully acknowledged for financial support.

REFERENCES

[1] S. Martinuzzi, O. Palais, M. Pasquinelli, F. Ferrazza, Eur. Phys. J. Appl. Phys., 32 (2005), 187-192.
[2] A. Cuevaes, M. J. Kerr, C. Samundsett, F. Ferrazza, G. Coletti, Appl. Phys. Lett., 81 (2002), 4952.
[3] D. Macdonald, J. L. Geerligs, in 19th European Photovoltaic Solar Energy Conference, (2004)
[4] J. Libal, T. Buck, R. Kopecek, P. Fath, K. Wambach, M. Acciarri, S. Binetti, L. J. Geerligs in 19th European Photovoltaic Solar Energy Conference, (2004), 1013.
[5] C. Schmiga, H. Nagel, S. Stechemetz, R. Hezel, in 19th European Photovoltaic Solar Energy Conference, (2004), 1060.
[6] M. Acciarri, S. Binetti, A. Le Donne, S. Marchionna, M. Vimercati, J. Libal, R. Kopecek, K. Wambach, Prog. Photovolt. Res. Appl., 15 (2007), 375–386.
[7] E. Olsen, E. J. Ørelid, in in 21th European Photovoltaic Solar Energy Conference (2006).
[8] Kittler M, Ulhaq-Bouillet C, Hersener J, Schaeffler F. Solid St. Phenom., 32 (1993), 559.
[9] ASTM F 1188-93a, Standard test method for interstitial atomic oxygen content of silicon by infrared absorbtion, (1993), 438-441.
[10] STM F1391-93 Standard Test Methods for substitutional atomic carbon content of silicon by infrared absorbtion, (1993).
[11] LECO Corporation, Application Bulletin, (1991).
[12] ASTM F76-86, Standard Test Methods for Measuring Resistivity and Hall Coefficient and Determining Hall Mobility in Single-Crystal Semiconductors, (2002).
[13] ASTM F43-99, Standard test methods for resistivity of semiconductor materials, (1999), ASTM Int. USA.
[14] S. Martinuzzi, I. Perichaud, O. Palais, Solar Energy Materials & Solar Cells, 91 (2007), 1172–1175.
[15] J. Chen, T. Sekiguci, D. Yang, F. Yin, K. Kido, S. Tsurekawa, J. Applied Physics, 96 (2004), 5490-5495.
[16] V. Kveder, M. Kittler, W. Schroter, Physical Review B, 63 (2001).

[17] G. Davies, Physics Reports, 176 (1989), 83.
[18] W. Kürner, R. Sauer, A. Dornen, K. Thonke, Phys. Rev. B, 39 (1989), 13327.
[19] S. Pizzini, S. Binetti, E. Leoni, A. Le Donne, M. Acciarri, A. Castaldini, Mat. Res. Soc. Symp. Proc., (2002), 692.
[20] J. Weber, H. J. Queisser, MRS Symp. Proc., 59 (1986), 147.
[21] S. Binetti, J. Libal, M. Acciarri, Unpublished work within EU project FoXy, 2007.